POLITECNICO DI TORINO
Repository ISTITUZIONALE

Single-state weighted particle filter with application to Earth Observation missions

Terms of use:

(Article begins on next page)

11 April 2024

Single-state weighted particle filter with application to Earth Observation missions

Cesare Donati [*,**] **Martina Mammarella** [**,1]
Fabrizio Dabbene [**]

* DET, Politecnico di Torino, Turin, Italy
(e-mail: cesare.donati@polito.it)
** CNR-IEIIT, Turin, Italy
(e-mail: martina.mammarella, fabrizio.dabbene@ieiit.cnr.it)

Abstract: To push the boundaries of autonomy in space, the spacecraft must rely on its own sensors to achieve positioning and environmental perception. In this context, the key problem of autonomous navigation is the nonlinear state estimation of the spacecraft in a dynamic 3D environment. In this paper, we propose a new approach based on a single-state sub-partitioning of the state vector and a partial updating of the vector of weights according to the specific information provided by each sensor. In this way, we avoid to lose information in the resampling phase thanks to a parallelization approach. The proposed method has been applied to an Earth observation mission and the efficacy of the proposed approach is demonstrated with a numerical example using a high-fidelity orbital simulator.

Keywords: Aerospace; particle filtering; information and sensor fusion; guidance, navigation and control of vehicles; high accuracy pointing

1. INTRODUCTION

In the pathway towards fully autonomous spacecraft, space systems shall be designed to operate in an unpredictable and partially unknown environment. In this framework, two main concepts result of particular relevance: i) *perception*, and ii) *navigation* Elkaim et al. (2015). The problem of sensor fusion in the aerospace field is typically handled exploiting Kalman-like filtering techniques, used to merge measurements provided by different sources (see e.g. Sasiadek and Hartana (2004); VanDyke et al. (2004); Markley and Sedlak (2008); Finance et al. (2021); Donati et al. (2022) and references therein). On the other hand, to accurately model the dynamics of complex systems, it becomes crucial to appropriately take into account *nonlinearity* and *non-Gaussian* probabilities.

In this context, a valid alternative is represented by the so-called particle filter (PF), which uses a set of particles (also called samples) to represent the posterior distribution of a stochastic process given the noisy and/or partial observations. For this category of filters, the state-space model can be nonlinear and the initial state and noise distributions can take any form required (not only Normal distributions). Several PF navigation filters have been proposed for space systems. Different PF-based techniques have been proposed (see e.g., Cheng and Crassidis (2004), Mashiku et al. (2012), Kiani and Pourtakdoust (2015), He et al. (2017), Bazik et al. (2019), Ning and Fang (2008)).

In PFs, the samples from the distribution are represented by a set of particles, each one with an assigned likelihood

weight, which represents the probability of that particle being sampled from the probability density function. A common problem in PFs is that, after few iterations, all but few particles tend to have *negligible* weights. In other terms, the estimation error's variance of particles will increase and many weights will take small values, thus not contributing to the final solution. As a result, only some samples will represent a reliable estimation, thus degrading PF performances. To overcome this issue, a resampling step is typically introduced after the update phase which outputs a new set of N_s particles starting from the original set, where each particle has a probability of being generated equal to its weight. This means that particles with higher weights are more likely to appear in the new set and could be chosen multiple times, while the number of particles from the lower weights is reduced. Because of the computational load of this step, in Hol et al. (2006) different resampling strategies have been analyzed and compared in terms of performances and computational requirements.

Despite the resampling technique, all the PFs share the same commonality: the larger is the number of samples, the better becomes the approximation of the posterior density function, the more accurate the estimation will be. For this reason, in the case of a system with an high number of state variables, an insufficient number of particles gives surely rise to a degeneracy problem and, more generally, to divergent and inaccurate estimations of the state vector. In particular, it is proven by Poterjoy (2016) that the number of particles required to accurately represent the a-posteriori densities increases exponentially with the dimension of the state space .

Peer review under responsibility of International Federation of Automatic Control.
10.1016/j.ifacol.2023.10.650

In recent years, some variants of the particle filter have been proposed, whose aim was to reduce the computational complexity of the filter for large state space dimensions. Some examples are the equivalent weight PF (Ades and van Leeuwen (2015)), the unweighted PF (Surace et al. (2020)), the adaptive PF (Soto (2005); Carmi and Oshman (2009)), and the variational Bayesian multiple PF Ait-El-Fquih and Hoteit (2016). Moreover, differently from conventional implementations of PFs, where for each particle a single weight based on the whole set of input measurements is generated, the multiple particle filter (MPF) (Poterjoy, 2016; Poterjoy and Anderson, 2016) and the multiple-weighting PF (MW-PF) (Zocca et al., 2022) variants derive multiple weights associated to sub-spaces/sub-partitions of the complete state-space. The process of choosing the correct states partitions as proposed in the MW-PF approach and simultaneously avoiding complex filtering structures (e.g. the communication phase introduced in the MPF) can be challenging, especially when different sensors provide information about same portions of the state space.

In this paper, we propose a single-state weighted PF (SSW-PF), which particularizes the MW-PF approach to the case of multiple sensors measuring interconnected portions of the state-space. Moreover, it introduces a MPF-like parallel structure in the resampling stage in order to avoid the loss of information present in this step of the MW-PF. The main aim of the SSW-PF is to maintain the simplicity of the weight computation of a standard PF, while defining a vector of weights where each element represents the importance of a single state variable. In this way, we obtain a one-dimension partitioning. Moreover, we pre-compute the weights for the state variable that cannot be directly observed by the sensors, reducing the computational burden for the weight update phase.

As case study, we selected an Earth observation (EO) mission performed by a pico-satellite, which shall guarantee fine pointing requirements. To prove the benefits achievable in terms of attitude estimation, we compared the SSW-PF with a standard PF scheme (Gustafsson (2010)) and an EKF (Donati et al. (2022)).

2. SINGLE-STATE WEIGHTED PARTICLE FILTER

Let us consider the (possibly) nonlinear dynamical system

$$x_{k+1} = f(x_k, u_k, v_k), \quad (1)$$

$$z_k^{(\ell)} = h^{(\ell)}(x_k) + \omega_k^{(\ell)}, \quad \ell \in [1, N_\ell] \subset \mathbb{N} \quad (2)$$

where $x_k \in \mathbb{R}^n$ is the state vector, $u_k \in \mathbb{R}^m$ is the command input, $v_k \in \mathbb{R}^n$ is the process noise caused by modeling approximations and model integration errors, $z_k^{(\ell)} \in \mathbb{R}^{\alpha_\ell}$ and $\omega_k^{(\ell)} \in \mathbb{R}^{\alpha_\ell}$ are the observation vector and the measurement noise related to the ℓ-th sensor, respectively. [2] Then, we define the vector of weights $w_k = [w_{k,1}, \ldots, w_{k,n}]^\top$, which represents the importance and reliability given to the estimation of the j-th element of the state x_k on the base of the sensor measurement. Now, we introduce the set $\boldsymbol{S_k} = \{s_k^1, \ldots, s_k^i, \ldots, s_k^{N_s}\}$ containing N_s particles where each s_k^i is defined by the couple $\{x_k^i, w_k^i\}$, where $x_k^i \in \mathbb{R}^n$.

---

[2] We assume that each sensor can observe $\alpha_\ell \leq n$ state variables.

Then, we define the vectors of simulated measurements for the i-th particle as

$$\mathbf{Z}_k^i = \left\{ h^{(1)}(x_k^i), \ldots, h^{(\ell)}(x_k^i), \ldots, h^{(N_\ell)}(x_k^i) \right\}. \quad (3)$$

To initialize the set of N_s particles, we first assign to each particle a uniform distribution of initial importance weights, i.e., considering the generic i-th particle, we have

$$w_{k,0}^i = \frac{1}{N_s} \mathbb{1}_n, \quad i \in [1, N_s] \subset \mathbb{N}, \quad (4)$$

where $\mathbb{1}_n$ is a n-elements, all-ones (column) vector. On the other hand, for the state $x_{k,0}^i$, we can use the previous knowledge on the initial condition of the considered system. For example, if the initial state $x_{k,0}$ of the system is exactly known, the starting samples can be distributed in a neighborhood of $x_{k,0}$. Then, as typical of PF approaches, the estimation process can be split into three phases, i.e. update, resampling, and propagation, which are described in details in the following sections.

2.1 Update phase

The main contribution of the proposed PF approach resides in the update phase. In particular, we introduce a specific weighting system, where the focus is on the single state variable instead on the overall particle as in the standard PF schemes. In this way, each particle is able to provide a higher-quality information because of the larger number of weights for each state, improving the accuracy of the final estimations. As we will show in the numerical simulations, this solution allows us to decrease the number of particles needed to obtain a given performance on the final estimation and, as a consequence, to reduce the computational complexity of the filter itself.

Specifically, the proposed approach aim at reducing the computational complexity of the update phase. To reach this objective, we implement a sensor-specific logic. We have that, for each i-th particle, the vector of weights w_k^i is updated on the base of the similarity between the simulated measurements of the particles (3) and the true observations $\mathbf{z}_k^i = [z_k^{(1)}, \ldots, z_k^{(N_\ell)}]_i$ collected by the N_ℓ sensors and represented by vectors of updaters.

In particular, we define as $\Xi_\ell^i = [(\xi_1^i)_\ell, \ldots, (\xi_n^i)_\ell]^\top \in \mathbb{R}^n$ the vector of weight updaters related to the ℓ-th sensor and for the i-th particle such that

$$w_k^i = w_{k-1}^i \prod_{\ell=1}^{N_\ell} \Xi_\ell^i, \quad (5)$$

where the weight updater $(\xi_j^i)_\ell$ for the j-th state variable $x_{k,j}^i$ is set either:

- equal to the probability that the i-th particle could have observed the true measurement of $x_{k,j}^i$ given by the ℓ-th sensor, if the ℓ-th sensor observes the j-th state variable, or
- equal to 1 otherwise, i.e. if the ℓ-th sensor does not observe the j-th component of x_k^i.

Last, w_k^i is normalized such that the sum over the N_s particle is equal to one.

Remark 1. To evaluate the performance of the filter, one can compute the RMSE over all the particle estimations as classical of PF approaches, i.e.

$$RMSE_k = \sqrt{\frac{\sum_{i=1}^{N_s}(x_k - x_k^i)^2}{N_s}} \qquad (6)$$

Another possibility, typical of Kalman-like filters, is to first obtain a good overall estimation of x_k from $\boldsymbol{S_k}$ performing the weighted mean between all the samples states, i.e.

$$\hat{x}_k = \sum_{i=1}^{N_s} w_k^i \circ x_k^i, \qquad (7)$$

and then compute the estimation error as $\tilde{x}_k = x_k - \hat{x}_k$.

2.2 Resampling phase

In the resampling phase, we propose a state-oriented strategy that allow us to overcome the typical limitations of other PF schemes related to the degeneracy problem (Daum and Huang, 2011) and sample impoverishment (Pardal et al., 2015).

In particular, we start generating a new set of N_s particles from $\boldsymbol{S_k}$, where each state estimation $x_{k,j}^i$ has a probability of being generated proportional to its weight $w_{k,j}^i$. As a result, the elements with higher weights are more likely to appear in the new set of particles and could be chosen multiple times. Applying the systematic resampling approach presented by Hol et al. (2006), we first compute the (normalized) cumulative sum C_j^i of the weights for each j-th state variable of the sample i as

$$C_j^i = \sum_{s=1}^i w_{k,j}^s. \qquad (8)$$

Then, we generate N_s ordered numbers u_j^η

$$\begin{cases} u_j^\eta = \bar{u} = \mathcal{U}\left[0, \dfrac{1}{N_s}\right), & \eta = 1 \\ u_j^\eta = u_j^{\eta-1} + \dfrac{1}{N_s}, & 1 < \eta \le N_s \end{cases} \qquad (9)$$

used to determine the number of times that the j-th element of the i-th particle will be resampled, corresponding to the cardinality of H = $\{\eta \in [1, N_s] \,|\, u_j^\eta \in [C_j^{i-1}, C_j^i)\}$ with $C_j^0 = 0$. This implies that the estimated variables with higher weights (e.g. samples 2 and 4 in Fig. 1) will generate larger intervals corresponding to a higher probability to be resampled (two and three times, respectively).
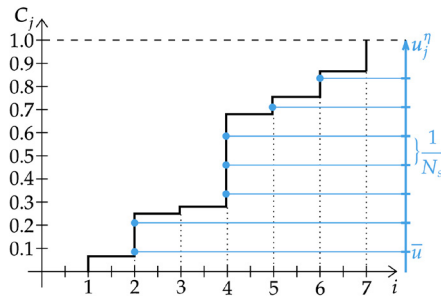

Fig. 1. Example of the systematic resampling approach.

2.3 Propagation phase

At each iteration k, the set of resampled particles is propagated at time $k+1$ according to (1), given u_k and

v_k^i. Note that, since the process noise is a random variable, the propagation phase is a stochastic operation and each particle is propagated considering a possible realization v_k^i of the random process noise v_k.

3. ONBOARD SENSORS MODELING

For the case study, we selected a pico-satellite whose attitude determination and control subsystem (ADCS) is composed by commercial-off-the-shelf magnetometers, gyroscopes, and Sun sensors. Moreover, we assume that the satellite is also equipped with a GPS sensor for estimating the satellite positioning. Being each sensor rigidly attached to the satellite frame, the measurements are defined in the satellite body frame. Then, these measurements are compared against model-generated estimates of their true values in the Earth Centered Inertial (ECI) frame. From the knowledge of at least two vectors expressed both in ECI and body-fixed frames, the attitude of the satellite can be estimated using the well-known TRIAD method (Black (1964)). In the follows, a brief review of the models used to simulate their output is reported. More details can be found in Wertz (2012); Markley and Crassidis (2014).

3.1 Gyroscope

The gyroscope provides measurements of the satellite angular velocity. A widely used three-axis continuous-time mathematical model for a rate-integrating gyroscope is described in (Tam (2015)) and reported hereafter

$$\tilde{\omega}_b = \omega_b + \beta_\omega + \eta_\omega, \qquad (10)$$

where $\tilde{\omega}_b$ is the measured angular rate, ω_b is the true angular velocity and η_ω is a zero-mean, Gaussian white noise with standard deviation σ_ω. The gyro bias β_ω changes over time as $\dot{\beta}_\omega = \eta_\beta$ where η_β is a zero-mean, Gaussian white noise with standard deviation σ_β. To initialize the bias term β_ω^0 when the gyroscopes are turned on, we use a different Normal distribution with standard deviation σ_{β_0}, i.e. $\beta_\omega^0 \sim \mathcal{N}(0, \sigma_{\beta_0}^2)$. Note that η_ω, η_β, and β_ω^0 are independent. Then, using the quaternion kinematics equation, it is possible to recover the estimated satellite orientation (see Markley and Crassidis (2014)).

3.2 Magnetometer

Magnetometers measure the strength and direction of the local magnetic field. Knowing the position of the satellite, it is possible to generate a true inertial magnetic field vector b_{mag}^I by using the International Geomagnetic Reference Field model Alken et al. (2021) of the Earth's magnetic field. Then, the magnetometer output is

$$\tilde{b}_{mag}^B = b_{mag}^B + \beta_{mag} + \eta_{mag}. \qquad (11)$$

where $\tilde{b}_{mag}^B$ is the measured magnetic field in the body frame, β_{mag} is the magnetometer bias, and η_{mag} is a zero-mean, Gaussian noise with standard deviation σ_{mag}. Then, as described by Bergamasco and Lovera (2013), it is possible to recover the satellite orientation using any method to solve the spacecraft attitude determination problem and compute the rotation matrix R_I^B such that $\tilde{b}_{mag}^B = R_I^B b_{mag}^I$.

3.3 Sun sensor

The Sun sensor is a navigational instrument used by spacecraft to detect the position of the Sun in terms of azimuth and elevation angles. Let assume we know the ECI Sun-Earth position, computed as described by Vallado (2001), and the ECI satellite position with respect to Earth, which is provided by the GPS, so that we can compute the relative ECI position among the satellite and the Sun r_{sun}^I. Then, we convert this vector to body coordinates r_{sun}^B using the attitude matrix and we compute azimuth az and el as described by Markley and Crassidis (2014). The measured azimuth and elevation can be recovered by adding white noise to the true values as $\tilde{az} = az + \eta_{az}$ and $\tilde{el} = el + \eta_{el}$, where η_{az} and η_{el} are zero-mean, Gaussian noises with standard deviations σ_{az} and σ_{el}, respectively. Last, we can recover the measured Sun unit vector $\tilde{r}_{sun}^B$ as

$$\tilde{r}_{sun}^B = \frac{1}{\sqrt{1 + \tan^2 \alpha + \tan^2 \beta}} \begin{bmatrix} \tan\alpha \\ 1 \\ \tan\beta \end{bmatrix}, \quad (12)$$

where $\tan\alpha = \tan\tilde{el}\sin\tilde{az}$ and $\tan\beta = \tan\tilde{el}\cos\tilde{az}$.

3.4 GPS

With a GPS receiver, it is possible to measure the orbital position and velocity of a satellite, and its model is defined as $\tilde{r}_{gps}^I = r_{gps}^I + \eta_r$ and $\tilde{v}_{gps}^I = v_{gps}^I + \eta_v$, where η_r and η_v represent the zero-mean, Gaussian white noises affecting the inertial position and velocity vectors with standard deviations σ_r and σ_v, respectively.

3.5 Attitude determination method

Knowing at least two vectors expressed both in ECI and body-fixed frames, one possibility to estimate the satellite attitude is the well-known TRIAD method (Black (1964))[3]. Given the magnetic field vectors b_{mag}^I, b_{mag}^B and the Sun vectors r_{sun}^I, r_{sun}^B, the TRIAD algorithms provides the direction cosine matrix (DCM) relating the two frame as follows:

(1) we compute the rotation matrix $R_t = [\hat{t}_{1,i} \, \hat{t}_{2,i} \, \hat{t}_{3,i}]$ from the i-the frame to the intermediate frame T as

$$\hat{t}_{1,i} \equiv \frac{r_{sun}^i}{\|r_{sun}^i\|}, \, \hat{t}_{2,i} \equiv \frac{r_{sun}^i \times b_{mag}^i}{\|r_{sun}^i \times b_{mag}^i\|}, \, \hat{t}_{3,i} \equiv \hat{t}_{1,i} \times \hat{t}_{2,i};$$

(2) we obtain the T-to-B R_t^B and T-to-I R_t^I DCMs;
(3) we recover the ECI-to-body DCM as $R_I^B = R_t^B (R_t^I)^\top$.

4. NUMERICAL RESULTS

As test case, we considered a 3U CubeSat with a mass of 4 kg, orbiting on an equatorial, 400 km circular orbit. The ADCS relies on the SSW-PF estimator for attitude estimation and on a PID controller for guaranteeing the desired pointing requirement for a Earth-pointing mission. Consequently, for the specific case study, the yaw angle ψ has been the only variable controlled. The time frame for all test cases is a half-orbital period.

---

[3] It is also possible to use alternative attitude determination algorithms e.g., the Q-Method.

The attitude dynamics of the satellite in the body frame is modeled using the standard Euler equations, in which we also included the RWs contribution, i.e.

$$J\dot{\omega}_B = M - \omega_B \times (J\omega_B + J_{RW}\omega_{RW}) \quad (13)$$

with $\omega_B = [\omega_x \, \omega_y \, \omega_z]^\top$ the satellite angular velocity in the body frame, J the satellite inertia tensor, M the sum of control torque and environmental disturbances (i.e., drag, gravity gradient, solar pressure), and J_{RW} and ω_{RW} the inertial and angular rate of the RWs, respectively. Then, the satellite orientation defined by the quaternion $q = [q_s \, q_v]^\top = [q_s \, q_1 \, q_2 \, q_3]^\top$ can be computed integrating the kinematic equations, i.e.

$$\dot{q} = \frac{1}{2}\Sigma(q)\omega_B, \quad \Sigma(q) = \begin{bmatrix} -q^\top \\ q_S \mathbb{I}_3 + [q]_\times \end{bmatrix}. \quad (14)$$

The results presented in this section focus on highlighting the improvements achievable exploiting the proposed SSW-PF approach compared with an EKF and a classical PF on three main aspects: i) estimation accuracy over the state variables; ii) average/ maximum estimation error, number of particles being equal for the PFs; and iii) computational cost.
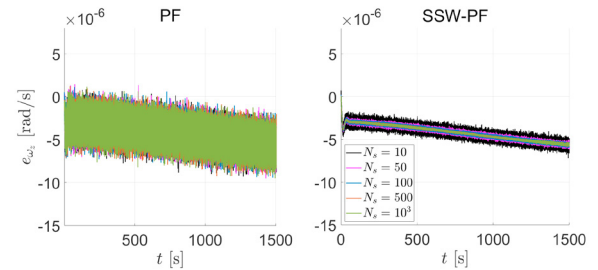

Fig. 2. Estimation error for different N_s using PF and SSW-PF.

We start analyzing the estimation error for one of the angular velocity components, i.e. ω_z, comparing the performance achieved applying the proposed SSW-PF and a classical PF for different number of particles N_s. In Figure 2, we can observe that the average estimation error e_{ω_z} is almost constant, despite the filtering approach adopted and the number of particles. On the other hand, we show that better performance in terms of variance can be achieved when the SSW-PF is exploited. In particular, when we apply the SSW-PF, if we increase the number of particles from $N_s = 10$ up to $N_s = 10^3$, we can spot a reduction in the estimation error variance, with a decrease inversely proportional to the increase of the samples. On the other side, the variance for the classical PF is less sensitive to the increment of N_s. These results are also reported in Table 1 in terms of standard deviation σ_{ω_z}, confirming the different effect of increasing N_s over the two PF schemes.

N_s	10	50	100	500	1000
SSW [μrad/s]	0.6499	0.5852	0.5767	0.5703	0.5691
PF [μrad/s]	1.1425	1.1459	1.1431	1.1431	1.1464

Table 1. Standard deviation σ_{ω_z} for various N_s.

Next, we focus on comparing the performance of the two PFs exploiting the same number of particles, i.e. $N_s = 10$. Fig. 3 shows the effectiveness of the proposed approach (lavender line) with respect to a classical PF (black line).
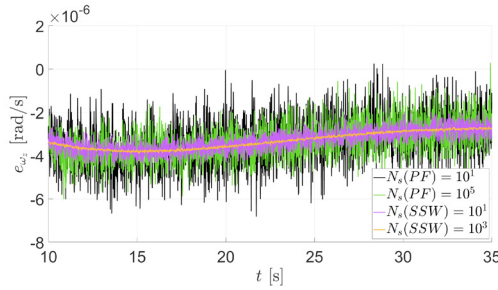
Fig. 3. Comparison of PF and SSW-PF in terms of e_{ω_z}.

In particular, we are able to reduce the variance of about one order of magnitude, from $1.3052 \cdot 10^{-12}$ achieved with the PF to $4.2249 \cdot 10^{-13}$ obtained with the SSW-PF. In this figure, we can also value the improvements attained increasing N_s up to 10^3 (orange line). On the other hand, to reach performance comparable with the SSW-PF but using a classical PF, we need to increase the number of particles up to 10^5 (green line). In this way, we obtain similar results in terms of average (SSW-PF: $-3.6877 \cdot 10^{-06}$/ PF: $-3.0163 \cdot 10^{-06}$) and maximum (SSW-PF: $5.8052 \cdot 10^{-06}$, PF: $6.0104 \cdot 10^{-06}$) estimation error, and variance (SSW-PF: $1.3052 \cdot 10^{-12}$, PF: $1.1685 \cdot 10^{-12}$).
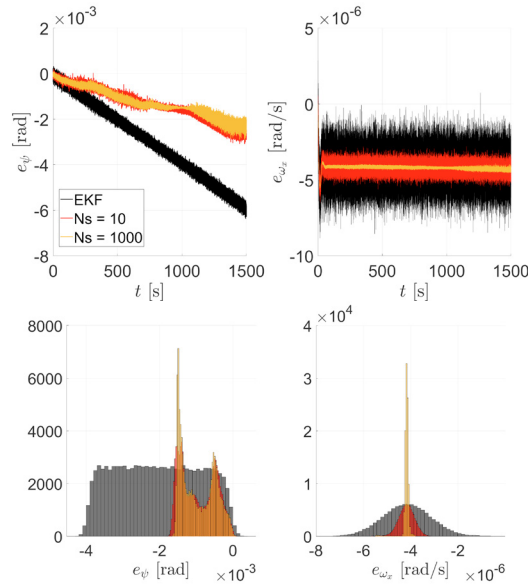

Fig. 4. Estimation error and error distribution for ψ (left) and to ω_x (right) using EKF and SSW-PF.

Then, we compare the performance of the SSW-PF (for $N_s = 10$ and $N_s = 10^3$) against a standard EKF for two different state variables, as shown in Fig. 4: the controlled variable ψ (left) and the angular rate ω_x (right).

Starting from the analysis of the Euler angle ψ, we can observe in the top figure how the EKF introduces an estimation error, which is drifting away from zero. On the other hand, the lower estimation error achieved with the SSW-PF allows to obtain a more accurate pointing. Nonetheless, it is worth to highlight that both approaches are able to achieve a pointing error lower than 1 deg.

Focusing on the corresponding estimation error distribution plot (bottom left), we can spot two picks for the SSW-PF, one corresponding to the process noise (around 10^{-3}) and the other one shifted by the average estimation

error (i.e. 10^{-3}). On the other hand, the EKF presents an almost uniform distribution. In neither case, we can observe the typical normal distribution. This is due to the non-gaussianity introduced by sensors modeling and the triad method. Moreover, this plot highlights how the SSW-PF, and more in general the PF schemes, can handle also non-Gaussian distributions without compromising the filtering efficacy, unlike Kalman-like approaches.

On the other side, we analyze the evolution of the estimation error and variance related to ω_x. Here, we can notice that the average error is comparable (around $4 \cdot 10^{-6}$) among the two approached whereas the variance is significantly reduced applying the SSW-PF, especially when $N_s = 10^3$. Moreover, we can observe that all three estimation error distributions present a Gaussian distribution but with a bias introduced by the random-walk term in the gyroscope modelling, which shifts the bell curves from zero to the mean error.

The last aspect analyzed is the correlation among the number of particles and the computation time for the PF schemes. To compare the performance of the proposed scheme with respect to a classical one, we performed different simulations, each one with the same length, i.e. 150 s, but different N_s up to 10^3. As shown in Fig. 5, despite the exploited approach, the larger the number of samples is, the higher the computation time (red line) required to complete a full simulation will be. However, with the same N_s, the PF approach (blue dashed line) is less computational demanding than the proposed SSW-PF, in particular for large N_s. Moreover, we can observe that for $N_s < 900$, the simulation time is higher than the SSW-PF computation time. While, if we further increase the number of particles, the real-time implementability could be not attained. On the other hand, the PF is more effective from a computational viewpoint, at the expense of worsened estimation accuracy.
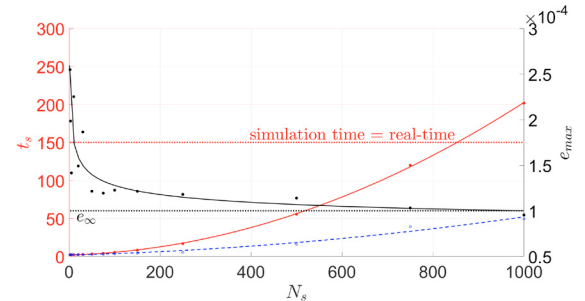

Fig. 5. Computation time with respect N_s for the SSW-PF (red) and a classical PF (blue), overlapped with the evolution of the maximum estimation error e_∞ achieved with the SSW-PF for different N_s.

A similar trade-off also characterizes the EKF where a (much) faster algorithm provides degraded estimation performance. In Fig. 5, we also report the maximum estimation error e_{max} (black line) with respect to N_s, and we can observe an exponential trend where the lower the number of samples, the larger the estimation error. Moreover, we can observe that the maximum estimation error is converging to a steady-state value e_∞ (black dotted line), which corresponds to the process noise included into the propagation phase, i.e. 10^{-4}. Overlapping these

two trends, we can conclude that one could select the desired estimation accuracy and, correspondingly, identify the (minimum) number of particles to be exploited to guarantee not only the required performance but also the real-time implementation of the proposed filtering scheme.

5. CONCLUSIONS

In this paper, we presented an innovative multiple weight particle filter that allows to fuse data from heterogeneous sensors with limited computational complexity. The sub-partitioning of the state-space is one-dimensional and the weights are partially pre-defined according to the measured states. The efficacy with respect to classical particle and Kalman filtering techniques was shown for an Earth orbit mission of a pico-satellite. The results showed that better estimation performance can be achieve at the expense of a higher computational cost, while improving the estimation accuracy with a much lower number of particles with respect to classical PF schemes.

REFERENCES

Ades, M. and van Leeuwen, P.J. (2015). The equivalent-weights particle filter in a high-dimensional system. *Quarterly Journal of the Royal Meteorological Society*, 141, 484–503.

Ait-El-Fquih, B. and Hoteit, I. (2016). A variational Bayesian multiple particle filtering scheme for large-dimensional systems. *IEEE Transactions on Signal Processing*, 64(20), 5409–5422.

Alken, P., Thébault, E., Beggan, C.D., Amit, H., Aubert, J., Baerenzung, J., Bondar, T., Brown, W., Califf, S., Chambodut, A., et al. (2021). International geomagnetic reference field: The thirteenth generation. *Earth, Planets and Space*, 73(1), 1–25.

Bazik, M., Flewelling, B., Majji, M., and Mundy, J. (2019). Bayesian inference of spacecraft pose using particle filtering. *CoRR*, abs/1906.11182.

Bergamasco, M. and Lovera, M. (2013). Spacecraft attitude control based on magnetometers and gyros. In *2nd CEAS Specialist Conference on Guidance, Navigation & Control*, 1122–1137.

Black, H.D. (1964). A passive system for determining the attitude of a satellite. *AIAA journal*, 2(7), 1350–1351.

Carmi, A. and Oshman, Y. (2009). Adaptive particle filtering for spacecraft attitude estimation from vector observations. *Journal of Guidance, Control, and Dynamics*, 32(1), 232–241.

Cheng, Y. and Crassidis, J. (2004). Particle filtering for sequential spacecraft attitude estimation. In *AIAA guidance, navigation, and control conference and exhibit*.

Daum, F. and Huang, J. (2011). Particle degeneracy: Root cause and solution. In *Signal Processing, Sensor Fusion, and Target Recognition XX*, 367–377.

Donati, C., Mammarella, M., Comba, L., Biglia, A., Gay, P., and Dabbene, F. (2022). 3D distance filter for the autonomous navigation of UAVs in agricultural scenarios. *Remote Sensing*, 14(6), 1374.

Elkaim, G., Lie, F., and Gebre-Egziabher, D. (2015). Principles of guidance, navigation, and control of UAVs. *Handbook of Unmanned Aerial Vehicles*, 347–380.

Finance, A., Dufour, C., Boutéraon, T., Sarkissian, A., Mangin, A., Keckhut, P., and Meftah, M. (2021). In-orbit attitude determination of the UVSQ-SAT cubesat using TRIAD and MEKF methods. *Sensors*, 21(21).

Gustafsson, F. (2010). Particle filter theory and practice with positioning applications. *IEEE Aerospace and Electronic Systems Magazine*, 25(7), 53–82.

He, Y., Liang, B., He, J., and Li, S. (2017). Non-cooperative spacecraft pose tracking based on point cloud feature. *Acta Astronautica*, 139, 213–221.

Hol, J.D., Schön, T.B., and Gustafsson, F. (2006). On resampling algorithms for particle filters. *Nonlinear Statistical Signal Processing Workshop 2006*, 79–82.

Kiani, M. and Pourtakdoust, S.H. (2015). Adaptive square-root cubature–quadrature Kalman particle filter via KLD-sampling for orbit determination. *Aerospace Science and Technology*, 46, 159–167.

Markley, F.L. and Crassidis, J.L. (2014). *Fundamentals of spacecraft attitude determination and control*. Springer.

Markley, F.L. and Sedlak, J.E. (2008). Kalman filter for spinning spacecraft attitude estimation. *Journal of guidance, control, and dynamics*, 31(6), 1750–1760.

Mashiku, A., Garrison, J., and Carpenter, J.R. (2012). Statistical orbit determination using the particle filter for incorporating non-Gaussian uncertainties. In *AIAA/AAS Astrodynamics Specialist Conference*, 5063.

Ning, X. and Fang, J. (2008). Spacecraft autonomous navigation using unscented particle filter-based celestial/Doppler information fusion. *Measurement Science and Technology*, 19(9).

Pardal, P.C.P.M., Kuga, H.K., and de Moraes, R.V. (2015). The particle filter sample impoverishment problem in the orbit determination application. *Mathematical Problems in Engineering*, 2015.

Poterjoy, J. (2016). A localized particle filter for high-dimensional nonlinear systems. *Monthly Weather Review*, 144, 59–76.

Poterjoy, J. and Anderson, J.L. (2016). Efficient assimilation of simulated observations in a high-dimensional geophysical system using a localized particle filter. *Monthly Weather Review*, 144(5), 2007–2020.

Sasiadek, J.Z. and Hartana, P. (2004). GPS/INS sensor fusion for accurate positioning and navigation based on Kalman filtering. *IFAC Proceedings Volumes*, 37(5), 115–120.

Soto, A. (2005). Self adaptive particle filter. In *IJCAI*, 1398–1406. Citeseer.

Surace, S.C., Kutschireiter, A., and Pfister, J.P. (2020). Asymptotically exact unweighted particle filter for manifold-valued hidden states and point process observations. *IEEE Control Systems Letters*, 4, 480–485.

Tam, M.H.T. (2015). An attitude determination and control system for small satellites.

Vallado, D.A. (2001). *Fundamentals of astrodynamics and applications*, volume 12. Springer Dordrecht.

VanDyke, M.C., Schwartz, J.L., Hall, C.D., et al. (2004). Unscented Kalman filtering for spacecraft attitude state and parameter estimation. *Advances in the Astronautical Sciences*, 118(1), 217–228.

Wertz, J.R. (2012). *Spacecraft attitude determination and control*, volume 73. Springer Science & Business Media.

Zocca, S., Guo, Y., Minetto, A., and Dovis, F. (2022). Improved weighting in particle filters applied to precise state estimation in GNSS. *Frontiers in Robotics and AI*, 9.